Eur. Phys. J. D **41**, 281–286 (2007)
DOI: 10.1140/epjd/e2006-00233-9

THE EUROPEAN PHYSICAL JOURNAL D

K-shell ionization cross section of aluminium induced by low-energy highly charged argon ions*

X.M. Chen[1,a], J.X. Shao[1], Z.H. Yang[2], H.Q. Zhang[1], Y. Cui[1], X. Xu[1], G.Q. Xiao[2], Y.T. Zhao[2], X.A. Zhang[3], and Y.P. Zhang[2]

[1] Department of Modern Physics, Lanzhou University, Lanzhou 730000, P.R. China
[2] Institute of Modern Physics, the Chinese Academy of Science, Lanzhou 730000, P.R. China
[3] The Normal College of Xianyang, Xianyang 713000, P.R. China

Received 24 February 2006 / Received in final form 1st July 2006
Published online 20 October 2006 –

Abstract. Al K-shell X-ray yields are measured with highly charged Ar^{q+} ions (q = 12–16) bombarding against aluminium. The energy range of the Ar ions is from 180 to 380 keV. K-shell ionization cross sections of aluminium are also obtained from the yields data. The experimental data is explained within the framework of $2p\pi$-$2p\sigma$ rotational coupling. When Ar ions with $2p$-shell vacancies are incident on aluminium, the vacancies begin to reduce. Meanwhile, collisions against Al atoms lead to the production of new $2p$-shell vacancies of Ar ions. These Ar $2p$-shell vacancies will transfer to the $1s$ orbit of an Al atom via $2p\pi$-$2p\sigma$ rotational coupling leading to the emission of a K-shell X-ray of aluminiun. A model is constructed based on the base of the above physical scenario. The calculation results of the model are in agreement with the experimental results.

PACS. 32.80.Hd Auger effect and inner-shell excitation or ionization – 32.30.Rj X-ray spectra

1 Introduction

In recent decades, the interaction of multiply or highly charged ions with surfaces has been the subject of active research, which has profited from developments in ion-source technology for slow multiply and highly ionized atoms. The considerable amount of potential energy stored in those ions is liberated in collisions with solids in complex multi-electron processes [1]. These processes, in addition to the fundamental interest concerning the interaction mechanisms, are relevant with respect to practical aspects (e.g., plasma-wall interactions), and might have the potential for future technological applications (e.g., ion-beam modification and analysis of surfaces).

Most experimental work in this field has focused on measurements of X-rays of the projectile [2] and electron emission from the surface [3–5] and has led in recent years to significant progress in the understanding of the interaction mechanism [6,7]. The interaction between ions and metal in front of the surface is described by a classical "over-barrier" model [8]. Neutralization of the ions proceeds at rather large distances from the surface by resonant charge transfer of conduction band electrons into Rydberg levels of the projectiles, then at and below the surface plane, the inner shells will be filled in close encounters with target atoms to complete the relaxation sequence.

In this work, low energy ($v_1 \leq 1$ a.u.) Ar^{q+} ions (q = 12–16) impinging on the aluminium surface cause k-shell excitation of the target atoms. For this low energy and the near symmetric system, the perturbative theory of inner-shell ionization, such as perturbation-stationary-state (PSS) theory [9], is not appropriate, specifically in the collision regime of the molecular-orbit (MO) model. In the MO model, the projectile-target system is represented as a temporarily formed diatomic molecule characterized by the adiabatic, independent-particle orbits and energies. When the energy level of a molecular orbit containing a vacancy crosses, or is degenerate with, an initially lower energy level corresponding to a filled orbit, the vacancy can be transferred to this second orbit. After the collision partners separate, the transferred vacancy becomes an atomic inner-shell vacancy. The electron of Al $1s$ shell is promoted to Ar $2p$ shell via a coupling between the $2p\pi$-$2p\sigma$ states of the quasi-molecule. This coupling arises because the internuclear line, which is the axis of quantization of angular momentum, is rotating throughout the collision [10,11].

In order to obtain the theoretical X-ray yields of aluminium, the number of $2p$ vacancies and the kinetic energy

* Work supported by the Science and Technology Ministry Foundation of China (2002CCA00900) and the National Natural Science Foundation of China (10274088).

[a] e-mail: Chenxm@lzu.edu.cn

of argon ions at each depth from the target surface must be known. They determine the charge transfer cross sections of the $1s$ electrons of Al at each depth of the target. The theoretical X-ray yields of thick targets [12] will be obtained by integrating all these cross sections at each depth.

We report the experimental details in Section 2. Experimental data are analyzed in Section 3. The details of the calculation model we used are discussed in Section 4 and the theoretical results are compared to the experimental data in Section 5.

2 Apparatus and experiment method

The experimental set-up is schematically shown in Figure 1. The experiment was performed at the ECR ion source at the National Laboratory of the Heavy Ion Research Facility in Lanzhou. The details of the 14-GHz ECR ion source are described elsewhere [13].

Ar^{12+}–Ar^{16+} are extracted from the source at various high voltages, corresponding to projectile energies in the range 180 to 380 keV. The ions are selected by a 90° magnet. The beam is highly collimated by two sets of four jaw slits to a size of less than 2×2 mm^2. The beam intensity can be monitored to satisfy the experimental requirement. An electrometer coupled with a current integrator records the total charge deposited by the ion beam to an accuracy of ±5%. The target is set at 45° with respect to the ion beam axis and at 90° to line of sight of the X-ray detector in the chamber. The base pressure in the chamber is maintained at 2×10^{-8} mbar. The emitted X-rays transmit through a beryllium window which has a thickness of 50 μm and are detected by a Si (Li) detector outside the chamber. The detector has a solid angle of 5.5×10^{-3} sr and its energy resolution is about 190 eV at 5.9 keV. It is positioned as near as possible to the Be window to reduce the absorption of the air. The aluminum surface is cleaned and has a purity of 0.9999. The aluminum target has a size of 19×24 mm^2 and its thickness is 1 mm.

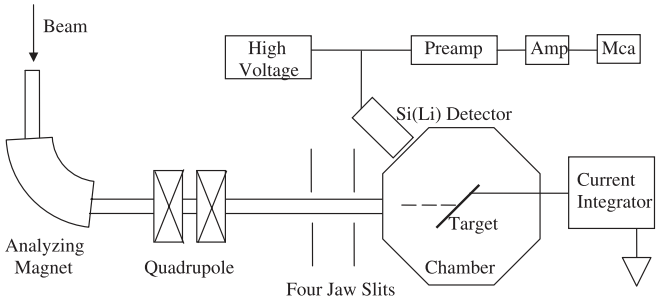

Fig. 1. Schematic diagram of the experimental set-up.

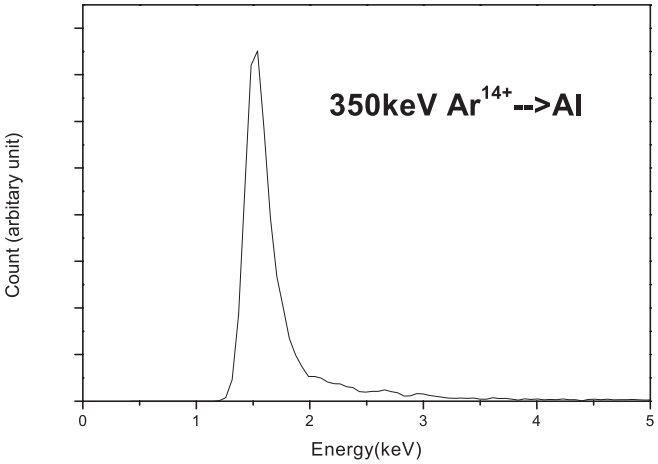

Fig. 2. Typical X-ray spectra of aluminium.

3 Data analysis

3.1 Thick target yield of K-shell X-ray

A typical X-ray spectrum of aluminium is presented in Figure 2. The Al K-shell X-ray yield per incident particle is:

$$Y(E) = \frac{N_X}{N_P} \frac{4\pi}{\Omega} \frac{1}{\varepsilon\mu} \tag{1}$$

N_X is the observed total X-ray counts, Ω is the solid angle of the X-ray detector seen from the target, ε is the detector efficiency, μ is the absorption coefficient of air and the beryllium window, N_P the total number of the incident particles.

We can integrate the counts in the Al (K) peak at 1.53 keV to determine the observed total Al K-shell X-ray counts N_X at projectile energy E. The values of N_X are extracted from the spectrum by computer fitting procedures. The detector efficiency ε is calculated using the manufacturer's specifications to include the effects of X-ray attenuation by the beryllium window, gold electrode layer, and silicon dead layer. The detector efficiency for Al (K) X-rays is calculated to be 38% for the detector with 25 μm windows respectively. The value of μ for 0.8 cm air and 50 μm beryllium window is 6.5×10^{-2}.

To decide the value of N_P, there is a problem of the secondary electrons emission. In 1993, Kurz and Aumayr gave experimental values for the total secondary electron yield from a clean gold surface by low energy Ar^{5+}–Ar^{16+} ions. In order to make the electron emission correction to the target Al, we measured the target currents of Al and Au from the electrometer under the condition of the same beam states (beam energy, charge state and beam intensity all the same). Let I be the true beam current intensity, I_{Al} the target current intensity of Al, I_{Au} the target current of Au

$$\frac{I_{\mathrm{Au}}}{1+\beta} = I = \frac{I_{\mathrm{Al}}}{1+\alpha} \tag{2}$$

α, β are the secondary electron emission coefficients for Al and Au, the value of β is taken from Kurz [14]. We can get the value of α from (2), then decide the true beam intensity and the value of N_P by the method of measuring the target current of Al and Au at the same time.

Our yield data excitated by various charge states of argon ions are shown in Figures 3–7. The yield data are

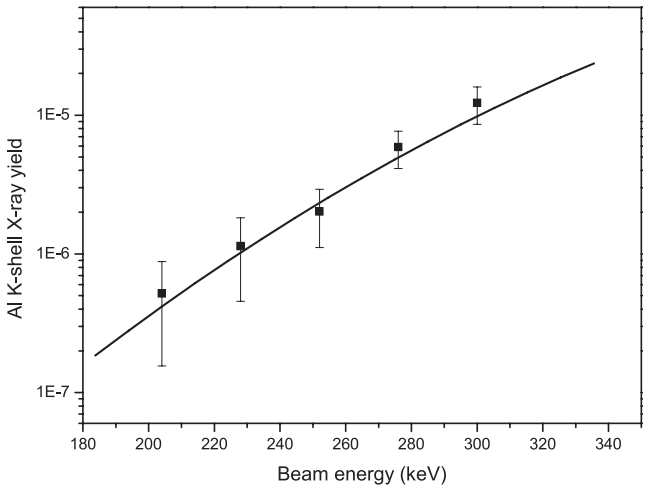

Fig. 3. Al K-shell X-ray yield by Ar^{12+}, the solid line is the theoretical results calculated by our model and the square dots are the experimental results.

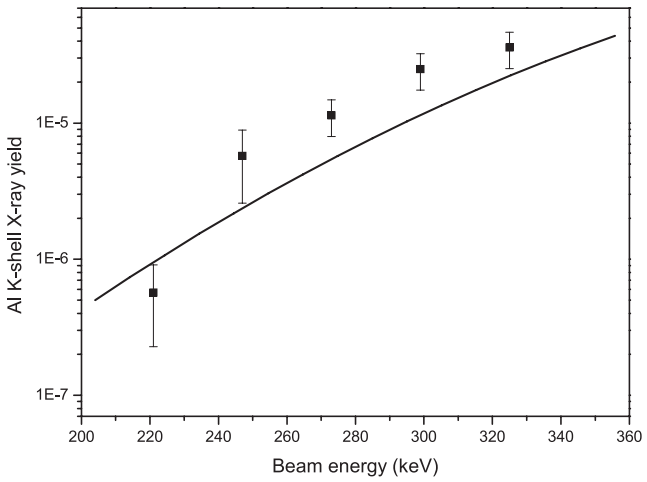

Fig. 4. Al K-shell X-ray yield by Ar^{13+}, the solid line is the theoretical results calculated by our model and the square dots are the experimental results.

plotted against beam energy, after corrections for background and dead time. The typical uncertainty of our yield data is ±25%, but for the low energy point, beam energy less than 240 keV, the uncertainty is ±55% due to the uncertainty of the background in the spectrum.

3.2 X-ray production cross section

We extract the X-ray production cross section from Y according to the standard formula

$$\sigma_X(E_1) = \frac{1}{N}\left[\left(\frac{dY}{dE}\frac{dE}{dR}\right)_{E1} + \overline{\mu}\frac{\cos\theta}{\cos\varphi}Y(E_1)\right] \quad (3)$$

where E_1 is the beam energy, N the target density, dE/dR is the stopping power, $\overline{\mu}$ the self-absorption coefficient of the target for its own characteristic X-ray. For these low

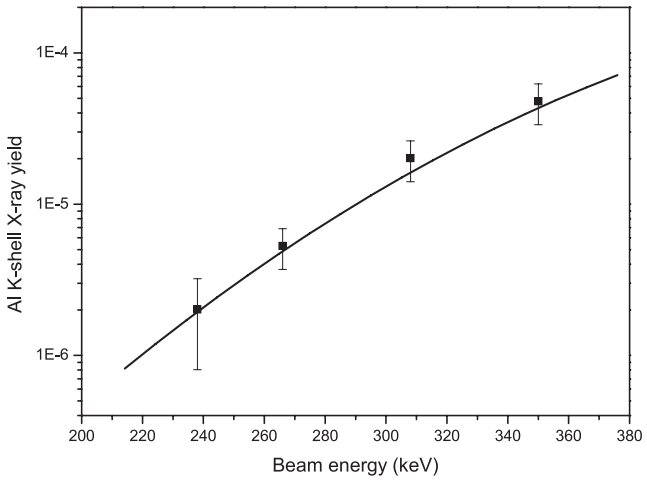

Fig. 5. Al K-shell X-ray yield by Ar^{14+}, the solid line is the theoretical results calculated by our model and the square dots are the experimental results.

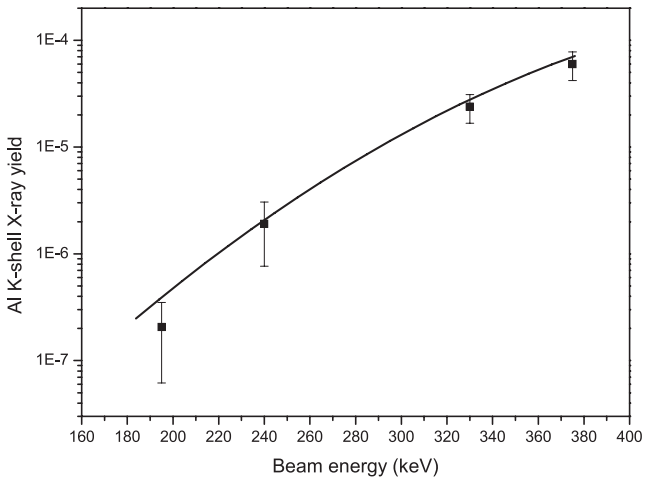

Fig. 6. Al K-shell X-ray yield by Ar^{15+}, the solid line is the theoretical results calculated by our model and the square dots are the experimental results.

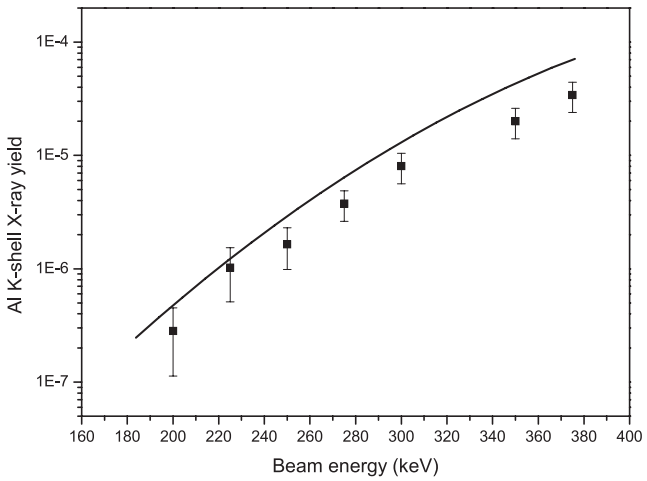

Fig. 7. Al K-shell X-ray yield by Ar^{16+}, the solid line is the theoretical results calculated by our model and the square dots are the experimental results.

beam energies of several hundred keV, we neglect the self-absorption effect. The stopping power data we used is the theoretical equations developed by Lindhard, Scharff, and Schiott [15], which has an uncertainty less than ±40%. Our yield curves allow differentiation with regard to energy, the typical uncertainty of the X-ray production cross section is ≤50% and ≤70% for the beam energy less than 240 keV.

Then we get the Al K-shell ionization cross section, $\sigma_I(E_1)$, for given beam energy E_1,

$$\sigma_I(E_1) = \omega_K^{-1}\sigma_X(E_1). \tag{4}$$

The value of $\omega_K = 0.04$ was taken from Fink et al. [16]. ω_K is the average K-shell fluorescent efficiency of Al. The plotted Al K-shell ionization cross sections σ_I against the incident beam energy E are shown in Figures 8–12, the theoretical results of ionization cross sections calculated by our model under the framework of $2p\sigma$-$2p\pi$ rotational coupling are also shown in Figures 8–12. The details of the model have been discussed in Section 4.

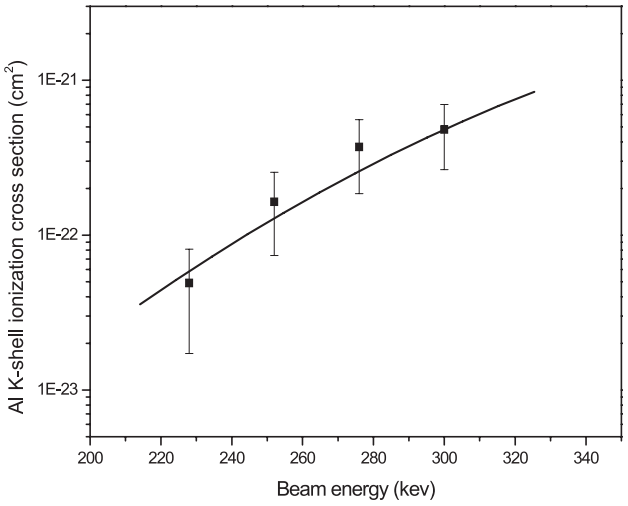

Fig. 8. Al K-shell ionization cross sections bombarded by Ar^{12+}, the solid line is the results calculated by our model and the square dots are the experimental results.

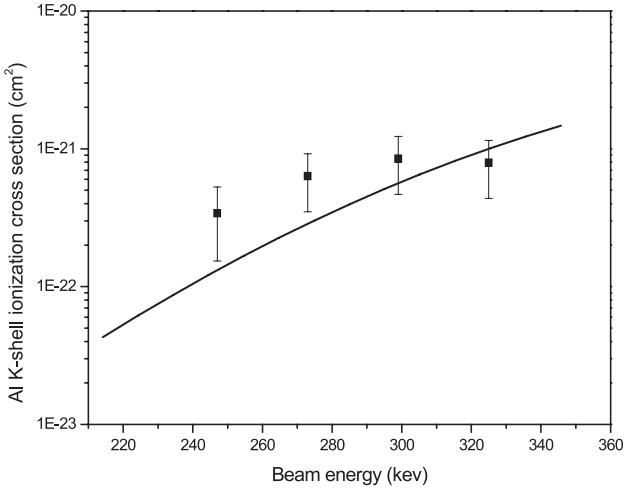

Fig. 9. Al K-shell ionization cross sections bombarded by Ar^{13+}, the solid line is the results calculated by our model and the square dots are the experimental results.

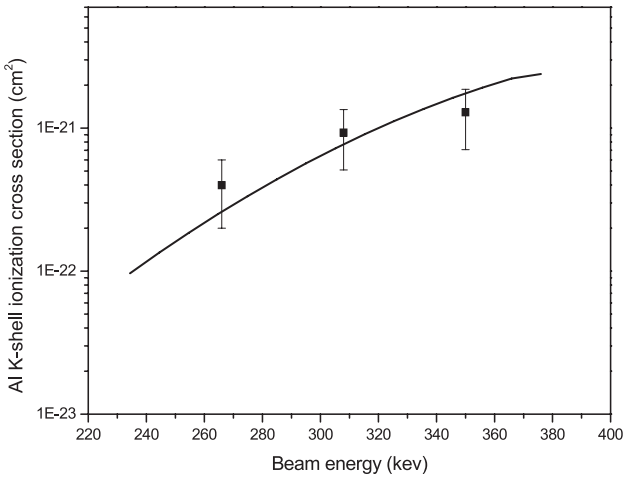

Fig. 10. Al K-shell ionization cross sections bombarded by Ar^{14+}, the solid line is the results calculated by our model and the square dots are the experimental results.

4 Calculation of the ionization cross section

4.1 Evolution of argon 2p vacancies

When Ar ions with $2p$-shell vacancies incident into aluminium, vacancies begin to reduce, meanwhile, with collision against Al atoms, new $2p$-shell vacancies of Ar ions are produced.

The number of $2p$ vacancies of argon, n, at a certain depth of the target is a function of the range R of incident ions and the residual range R^*, n satisfying the following equation:

$$\frac{dn(R,R^*)}{dR^*} = -\frac{n(R,R^*)}{v\,(R,R^*)\,\tau} + \sigma_{2P}^{\mathrm{Ar}} N \tag{5}$$

where τ is the lifetime of a $2p$ shell vacancy of argon. $\sigma_{2P}^{\mathrm{Ar}}$ is the ionization cross section of the $2p$ shell of argon, N the target density.

The solution of equation (5) is

$$\begin{aligned} n\,(R,R^*) &= n_0 \exp\left(-r/v(r)\tau\right) \\ &\quad + \sigma_{2P}^{\mathrm{Ar}} N v(r)\left[1-\exp\left(-r/v(r)\tau\right)\right] \end{aligned} \tag{6}$$

where $r = R - R^*$, n_0 is the number of the initial argon $2p$ vacancies.

4.2 2pπ-2pσ rotational coupling cross sections

The well-known equation for calculating the $2p\sigma$-$2p\pi_{X'}$ excitation cross section is:

$$\begin{aligned} \frac{dC_1}{dt} &= -\frac{bv}{R^2} f(R) C_2 \exp\left[i\int (E_1 - E_2)\,d\tau\right] \\ \frac{dC_2}{dt} &= \frac{bv}{R^2} f(R) C_1 \exp\left[-i\int (E_1 - E_2)\,d\tau\right]. \end{aligned} \tag{7}$$

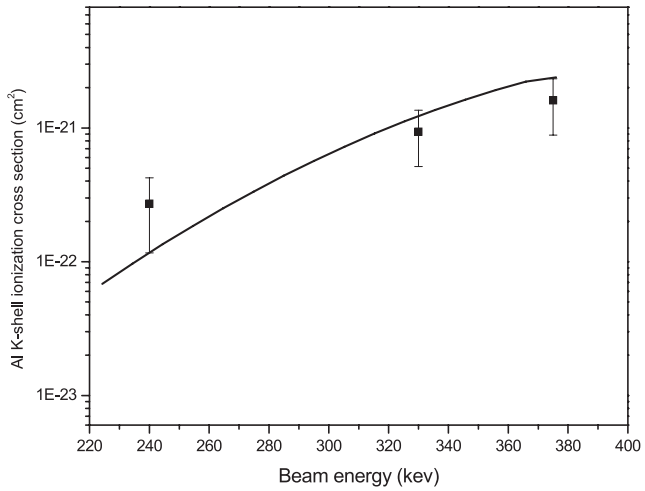

Fig. 11. Al K-shell ionization cross sections bombarded by Ar^{15+}, the solid line is the results calculated by our model and the square dots are the experimental results.

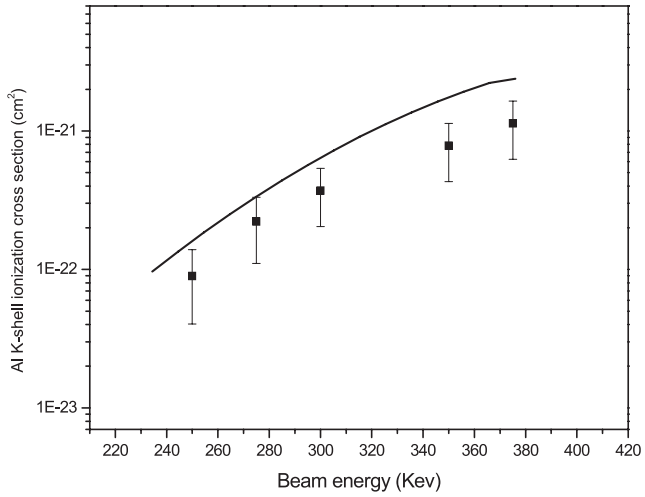

Fig. 12. Al K-shell ionization cross sections bombarded by Ar^{16+}, the solid line is the results calculated by our model and the square dots are the experimental results.

This equation describes the probability that one $2p\sigma$ electron transfers to one $2p\pi_{X'}$ vacancy, it is $P(b) = |c_2(+\infty)|^2$.

Briggs and Macek used this equation to solve the problem of a one vacancy collision system [17,18], such as the Ne^+ and O system.

In the present work, the $2p$ vacancies of argon ions are different at each depth of the target. This is the multi-electron and multi-vacancy process, we can construct the transfer probability of this multi-electron system using the single-electron probability $P(b)$ and the statistical factors.

In Section 4, we obtained the number of argon $2p$ vacancies at each depth of the aluminium target. On the basis of the above discussion, we can obtain the charge transfer cross section, $\sigma(R, R^*)$, of the multi-electron and multi-vacancy system.

The theoretical X-ray yield is

$$Y(E) = \int_0^R \sigma(R, R^*) dR^*,$$

then the ionization cross section is

$$\sigma_I(E) = (\omega_K N)^{-1} \frac{dY(E)}{dE} \frac{dE}{dR}.$$

dE/dR is the theoretical result of stopping power given by Lindhard [15].

Equation (7) is solved under three approximations:

(i) the Gershtein-Krivchenkov formula for the $2p\pi$-$2p\sigma$ energy gap is used: $E_1(R) - E_2(R) = kR^2$ where $k = 1/40 Z_1 Z_2 (Z_1 + Z_2)^2$;
(ii) the $2p\pi$-$2p\sigma$ radial overlap $f(R)$ is set equal to unity [17–19];
(iii) equations (7) are integrated along the screening Coulomb deflection trajectories, the screening potential function is $V = (Z_1 Z_2/r) \exp(-r/a)$, where a is the screening length discussed by Bohr [20].

4.3 Argon 2p-shell vacancy production

The value of $\sigma_{2P}^{\mathrm{Ar}}$ must be determined in order to obtain the calculated X-ray cross section, $\sigma_X(E)$.

We estimate the argon $2p$-shell ionization cross section using the binding-energy-modified BEA approximation.

According to the BEA theory, the vacancy production cross section is given by

$$\sigma_{BEA} = C\left(Z/U^2\right) f(v/U) \tag{8}$$

where C is the number of equivalent electrons having binding energy U, Z is the projectile atomic number, v is the velocity of the projectile.

Two electrons of the argon $2p$ shell will evolve to the $3d\sigma$ MO during the collision, the $3d\sigma$ MO will degenerate with the $3d\pi$ MO which evolved from the Al $2p$-state and the $3d\delta$ MO from the Ar $3d$-state. There is no direct coupling between the $3d\delta$ and $3d\sigma$ MO, and the $2p$-shell of aluminium contains no vacancy. The $2p$-shell electrons of argon will not be promoted to $3d\delta$ states directly, so the $2p$-shell vacancies of argon will be produced probably via direct ionization from the $3d\sigma$ MO. In an attempt to estimate the direct vacancy production of the argon $2p$-shell, the values of U, v, C, Z in equation (8) will be modified. $C = 2$ for two $3d\sigma$ electrons, the binding energy of the $3d\delta$ MO in the united atom (UA) limit, U_{3d}, is used instead of U, v is replaced by v_{Al}^C,the velocity of an aluminium atom in center of mass coordinates and $n = 3$. will be replaced by the effective charge Z_{eff}, an effective charge that the $3d\sigma$ electrons will feel from the moving aluminium nucleus

$$Z_{eff} \approx \frac{Z_2}{Z_1 + Z_2} Z_{3d} \tag{9}$$

where Z_1, Z_2 are the atomic numbers of Ar and Al, and Z_{3d} is the $3d$ level effective charge of the UA with binding

energy $U_{3d} = -Z_{3d}^2/2n^2 \approx 0.8$ a.u., $n = 3$. The analytic description of $\sigma_{2P}^{\mathrm{Ar}}$ is

$$\sigma_{2P}^{\mathrm{Ar}} = 2\left(Z_{eff}/U_{3d}^2\right) f\left(v_{\mathrm{Al}}^C/U_{3d}\right). \quad (10)$$

The theoretical Al K-shell X-ray yields and the K-shell ionization cross sections bombarded by Ar^{q+} ($q = 12$–16) ions calculated by this model are plotted in Figures 3–12 in order to compare with the experimental results.

5 Discussions

The experimental results indicate that with the same incident energy, Al K-shell X-ray yields, which are excited by Ar^{q+} ions with different charge states, are of the same order of magnitude. Nonetheless among them there are still some quantitative differences yield. The yields excited by Ar^{12+}, Ar^{14+} and Ar^{15+} are almost the same while the Ar^{13+} is larger and the Ar^{16+} yield is much smaller.

We assume that, for the same incident energy, two main factors will influence the charge transfer cross section of the Al 1s electrons; one is the available 2p shell vacancies of argon ions, the other is the energy gap between the 2$p\pi$ MO and the 2$p\sigma$ MO. The more vacancies, the larger the transfer cross section. The larger energy gap, the smaller the cross section will be.

From Ar^{12+} to Ar^{16+}, the number of available 2p vacancies varies from four to six. Meanwhile, more vacancies will decrease the screening strength among the electrons, which will increase the energy gap between 2$p\pi$ and 2$p\sigma$ orbits. The X-ray yields excited by Ar^{13+} are a bit larger than Ar^{12+}. In this case, the number of vacancies probably influences the cross section more strongly than the energy gap does. The yields excited by Ar^{14+}, Ar^{15+}, Ar^{16+} are all smaller than that of Ar^{13+}. In this case it may be that the energy gap influences the charge transfer cross section much more than the vacancies number does.

The yields excited by Ar^{15+} are a bit smaller than that of Ar^{14+} and the yields of Ar^{16+} are smaller than that of Ar^{15+}. The reason is that Ar^{14+} has two 2s electrons, Ar^{15+} has one, but Ar^{16+} has none. Meanwhile, these ions have the same number of 2p vacancies. So the conclusion is: the 2$p\pi$-2$p\sigma$ energy gap of Ar^{16+} is the largest and the energy gap of Ar^{14+} is the smallest, so the yields for Ar^{14+} will be the largest of the three, the yields for Ar^{16+} will be the smallest. This conclusion is in agreement with the results of the experiment.

The theoretical model is effective in estimating the magnitude of Al K-shell X-ray yields excited by Ar^{q+} ions ($q = 12$–16). But the model cannot describe the differences among the different charge states exactly. The model shows that the larger the charge states, and the more available vacancies there are, the larger the X-ray yields will be.

We solve equation (7) under the approximation that the energy gap between the 2$p\pi$ and 2$p\sigma$ states is described by the Gershtein-Krivchenkov approximation. This is a first order approximation. It is independent of the charge states of the ions, the second order differences for different charge states are neglected in this approximation. So, in our model the only factor that will influence the charge transfer cross section is the number of available vacancies. This is why the model describes the magnitude of the yields well but cannot describe the relative intensity between different charge states exactly.

References

1. P. Varga, Appl. Phys. A **44**, 31 (1987); P. Varga, Comm. At. Mol. Phys. **27**, 111 (1989)
2. J.P. Briand, L. de Billy, P. Charles, S. Essabaa, P. Briand, R. Geller, J.P. Desclaux, S. Bliman, C. Ristori, Phys. Rev. Lett. **65**, 159 (1990)
3. H. Kurz, K. Töglhofer, HP. Winter, F. Aumayr, R. Mann, Phys. Rev. Lett. **69**, 1140 (1992)
4. J. Das, L. Folkerts, R. Morgenstern, Phys. Rev. A **45**, 4669 (1992)
5. F.W. Meyer, S.H. Overbury, C.C. Havener, P.A. Zeijlmans wan Emmichoven, D.M. Zhner, Phys. Rev. Lett. **67**, 723 (1991)
6. J. Das, R. Morgenstern, Comm. At. Mol. Phys. **29**, 205 (1993)
7. F. Aumayr, HP. Winter, Comm. At. Mol. Phys. **29**, 275 (1994)
8. J. Burgdörfer, P. Lerner, F. Meyer, Phys. Rev. A **44**, 5674 (1991)
9. G. Basbas, W, Brandt, R.H. Ritchie, Phys. Rev. A **7**, 1971 (1973)
10. A. Russek, Phys. Rev. A **4**, 1918 (1971)
11. J.S. Briggs, J. Macek, J. Phys. B: At. Mol. Phys. **8**, 1909 (1975)
12. J.D. Gacia, R.J. Fortner, Rev. Mod. Phys. **45**, 111 (1973)
13. Z.M. Zhang et al. **27**, 914 (2003)
14. H. Kurz, F. Aumayr, C. Lemell, K. Töglhofer, H.P. Winter, Phys. Rev. A **48**, 2182 (1993)
15. J. Lindhard, M. Scharff, H.E. Schiott, Mat. Fys. Medd. Dan. Vid. Selsk. **33**, No. 14 (1963)
16. R.W. Fink, Rev. Mod. Phys. **38**, 513 (1966)
17. J.S. Briggs, Rep. Prog. Phys. **39**, 217 (1976)
18. R. Anholt, W.E. Meyerhof, A. Salin, Phys. Rev. A **16**, 951 (1977)
19. J.S. Briggs, J. Macek, J. Phys. B: At. Mol. Phys. **8**, 579 (1972)
20. N.Bohr, Kgl. Danske Videnskab. Selskab, Mat-fys. Medd. **18**, 8 (1948)